

Investigation of Inhibition Effect on Pathogen Microorganisms by Adding NPAg to Activated Carbon Obtained by Activating Hazelnut Shell with ZnCl₂

Birsen Sarıcı¹ , Esra Altıntığ^{2*} , Şükrü Karataş² 

¹ Düzce University, Faculty of Health Sciences, Department of Nutrition and Dietetics, Düzce, Türkiye, birsensarici@duzce.edu.tr, ror.org/04175wc52

² Sakarya University of Applied Sciences, Pamukova Vocational School, Department of Chemistry and Chemical Processing Technologies, Sakarya, Türkiye, altintig@subu.edu.tr, ror.org/01shwhq58

³ İstanbul Aydın University, Faculty of Engineering, Department of Food Engineering, İstanbul, Türkiye, sukrukaratas@aydin.edu.tr, ror.org/00qsyw664

*Corresponding Author

ARTICLE INFO

ABSTRACT

Keywords:

Activated carbon
Food safety
Hazelnut shell
Antimicrobial
NPAgAC

Article History:

Received: 17.03.2025

Revised: 13.05.2025

Accepted: 03.06.2025

Online Available: 19.06.2025

In this study, silver-coated activated carbon (NPAgAC) was obtained by adding nanoparticle silver (NPAg) to activated carbon (AC) produced from hazelnut shells by chemical activation and carbonization. SEM, FT-IR, and BET were evaluated. While the methylene blue (MB) number of the produced ACs was 490-499 mg/g, the MB numbers of NPAgAC were determined to be 421-453 mg/g. The iodine number of ACs was specified in the 1047-1612 mg/g range. The iodine numbers of NPAgACs were recorded in the 934-1022 mg/g range. Additionally, EDS and XRD analyses were performed on all samples. Well, diffusion and spreading plate methods were used to control the antimicrobial properties of the produced NPAgAC. The study used *Escherichia coli* (*E. coli*) and *Staphylococcus aureus* (*S. aureus*) as pathogenic microorganisms. In addition, the antimicrobial properties of NPAgACs were investigated using the spread plate method at various times and temperatures to determine their effectiveness in inhibiting the growth of *E. coli* in polluted waters. Studies have shown that hazelnut shells are a suitable starting material for producing activated carbon, and that NPAgAC exhibits high antimicrobial properties with food safety.

1. Introduction

As the global population is expected to reach 9.7 billion by 2050, concerns about food security are also on the rise [1]. Industrialization has also intensified water and environmental pollution, posing risks to public health and food safety [2]. Traditional methods and chemical preservatives are widely used to prevent food spoilage and control pathogens [1]. Although effective, the prolonged use of these chemicals has led to the accumulation of residues and the development of microbial resistance [2]. This has driven interest in safer, natural alternatives to conventional preservatives [3]. To mitigate existing water

pollution without harming human health, developed countries are focusing on utilizing agricultural waste as a source of biomass. This approach offers sustainable solutions to both waste management and water pollution prevention [4].

Activated carbons are substances with high adsorbent capacity produced by several special methods to obtain a larger surface area from various biomass and carbon-based materials [5]. Producing activated carbon from agricultural biomass waste, a low-cost raw material, has become increasingly common [3]. Biomass is a ubiquitous, low-cost, regularly produced

substance that does not pose a problem for a renewable environment [6]. Activated carbons are accepted as effective adsorbents for removing chemical pollutants in water due to their large surface area and highly porous structure [5]. However, activated carbons should possess bactericidal properties, depending on the location of use, as they can promote bacterial growth due to bacterial contamination, particularly in terms of biological compatibility with microorganisms [7].

Most nanoparticle atoms are unsaturated on the surface and, therefore, can easily bind to other atoms [8]. While the antibacterial effects of silver have been recognized since ancient times, the use of nanoparticulate silver (NPAg) in various applications has become increasingly common in recent years, owing to its antimicrobial properties and large surface area [9, 10]. Many nanomaterials, such as silver, have gained popularity in recent years, particularly for addressing the issue of antibiotic resistance and providing more economically sustainable public health conditions [11]. It attracts great attention due to its low toxicity [12]. Although the mechanisms underlying various morphological and structural changes caused by silver metal, silver ions, or NPAg ions in the cell walls of microorganisms are not yet fully understood, studies on this subject continue [11]. NPAg ions are thought to exert their antibacterial effect by binding to the bacteria's cell wall and cell membrane. It is believed that hydrogen cations alter this effect after they combine with functional thiol (-SH) groups in the proteins in the wall, deactivating them and reducing their permeability in the cell membrane, thereby causing the death of microorganisms [13, 14]. NPAg ions are preferred as antibacterial and antifungal due to their antimicrobial effects against fungi and bacteria [15, 16].

In the twenty-first century, as the world grapples with the climate change crisis, environmental pollution and wastewater management are among the most pressing problems [2]. Water is indispensable for all living things, and waste

from various industries, including textiles, food, health, and paper, pollutes water [3]. Efficient methods continue to be researched to remove substances that threaten the health of living things, such as pesticides, heavy metals, and dyestuffs, from wastewater [4]. Binding NPAg to activated carbon, which has a high adsorbent capacity, provides a vital solution for achieving antibacterial properties, reducing water pollution, improving food safety, and enhancing public health [8]. With its large surface area and varied pore sizes, activated carbon can be an excellent support material for NPAg [17].

This research focuses on the production of activated carbon using hazelnut shells, an agricultural waste material with an estimated annual yield of around 550,000 tons in Turkey. Approximately 50% of the total mass of harvested hazelnuts consists of shells. Despite their high carbon content, these shells are not sufficiently utilized as raw materials, posing a challenge to environmental sustainability [18]. Hazelnut shells, as a form of biomass, contain cellulose, hemicellulose, and lignin in varying proportions, making them a promising precursor for the production of activated carbon. Elemental analysis of lignocellulosic biomass has revealed an average carbon content of approximately 50%, indicating its value as a biomass feedstock [19]. Therefore, due to the favorable composition of its biocomponents, the production of activated carbon from hazelnut shells presents a viable solution for managing and disposing of agricultural waste, addressing an environmental concern, and generating a high-value product [20]. For this purpose, hazelnut shell was selected in our study.

For this purpose, the collected hazelnut shells were first purified through various pre-treatments. Washed and dried hazelnut shells were ground and separated into three mesh sizes (50-70-150). Samples chemically activated with $ZnCl_2$ in 3 different ratios (1:1, 1:2, 1:3) were carbonized in a tube furnace at 700 °C, and the produced activated carbons were stocked for characterization studies. The characterization

studies selected the activated carbon with the best efficiency.

Additionally, it seeks to enhance the properties of the produced activated carbon by incorporating NPAG to impart antimicrobial properties, offering a potential solution for inhibiting pathogens that threaten public health. NPAG was added to the best-activated carbon, as determined by SEM, FT-IR, and BET images, to enhance the antimicrobial effect. The Well diffusion method was used to test the antimicrobial effect of the obtained NPAGAC on *E. coli* and *S. aureus*, two pathogenic microorganisms.

2. General Methods

2.1. Materials and methods

The hazelnut shell samples used in this study were obtained at the end of the 2019 harvest season by mixing samples from merchant warehouses in the Giresun region with sample soda from six different points, according to TSE 3074 standards, and breaking the hazelnut kernels apart. The study utilized chemicals, including sodium alginate, $ZnCl_2$, $AgNO_3$ (purity > 99%), HCl, sodium hydrazine monohydrate, and NaOH, all sourced from Merck (Germany). All chemicals are analytical reagent grade.

Then, activated carbon production was completed with chemical activation and carbonization stages. The produced activated carbon was characterized, and antimicrobial studies were carried out.

2.2. Materials

In this research, all mixing operations were performed using a Wisestir MSH-20A magnetic stirrer. The materials were accurately weighed using a Precisa XB 220A analytical balance, and pH values were determined with a Mettler TOLEDO Seven Compact series pH meter. The carbonization of the activated carbon was conducted in a Proterm PTF 12 tubular furnace. A Nuve NS112 device supplied pure water for

the experiments. Shaking processes were conducted with a Nuve SL 350 shaker, and drying operations were performed using a Mido/2/AL brand oven. The determination of ash and moisture contents, along with wet chemical analyses, was carried out using a Nuve MF 100 drying oven.

Functional groups in HS, AC, and NPAGAC samples were identified using Fourier Transform Infrared Spectroscopy (FT-IR), performed on a PerkinElmer UATR-TWO instrument, covering the spectral range of 4000 to 400 cm^{-1} . The crystalline phases of AC and NPAGAC were examined using an X-ray diffractometer (XRD, Rigaku). Surface topography was investigated by a scanning electron microscope (SEM, Jeol JSM-6060 LV model). Specific surface area (m^2/g), pore diameter (nm), and volumes of micropores and meso-/macropores (cm^3/g) were assessed via multi-point Brunauer–Emmett–Teller (BET) analysis. Nitrogen adsorption measurements for pore structure and surface area evaluations were conducted using a Micromeritics ASAP 2020 analyzer under liquid nitrogen conditions at 77 K. Furthermore, MB adsorption experiments were analyzed with a Shimadzu UV-2600 UV-Visible spectrophotometer.

2.3. Production of activated carbon

Hazelnut shells taken after harvest were washed with tap and distilled water to purify them from impurities. They were dried at room temperature for 3 days and then in an oven at 60 °C for 3 days. For sizing, a mixer and a pulse mill were used in the grinding stage, and the material was sieved into three different mesh ranges (50, 70, and 150). The hazelnut shells were mixed with $ZnCl_2$, which was identified as a chemical activating agent, in three different ratios: 1:1, 1:2, and 1:3. After impregnating the ground hazelnut shells with $ZnCl_2$, they were shaken at 200 rpm for 24 h in a shaking incubator at 40°C for activation. In the next step, the excess of the chemical substance was filtered from the dense solution, and the samples were kept open at room temperature for one day under laboratory conditions.

The filtered mixtures were dried in an oven at 103 °C for 12 h. The samples were carbonized in a tube furnace at 800°C in a nitrogen atmosphere (flow rate, speed = 200 mL/min) with a heating rate of 10°C/min. At the end of the carbonization period, nitrogen flow continued until the furnace temperature dropped to 60 °C (approximately 24 h). To remove the ZnCl₂ from the activated carbon, it was first washed with 1 M HCl and then with distilled water until the pH reached 7. It was then allowed to dry in a 105°C oven for 12 h by filtration. Efficiency calculations were performed on the activated carbons obtained.

2.4. Production of NPAg and impregnation on AC

This study employed AgNO₃ as the precursor for the synthesis of NPAg. Solid AgNO₃ was dissolved in 100 mL of 25% by weight NH₃ at two different concentrations (0.5 g and 1 g). To achieve a homogeneous mixture, the solution was stirred at 150 rpm for 1 h at ambient temperature (298 K) using a magnetic stirrer. The synthesized diammine silver nitrate ([Ag(NH₃)₂]NO₃) solution was then placed into amber glass containers shielded with aluminum foil to protect from light exposure. The pH was adjusted to 9.0 using a nitric acid (HNO₃) solution. [2] The resulting NPAg solution was stored in light-proof containers wrapped with aluminum foil. Meanwhile, activated carbon (1g:1g) was prepared by combining it with sodium alginate (Sigma Aldrich) and stirring magnetically at 200 rpm for 60 min at room temperature.

While the biamin silver nitrate solution was prepared with a mixture of sodium alginate and activated carbon obtained in a three-necked glass balloon wrapped with aluminum foil, the solution was mixed simultaneously. Hydrazine monohydrate was then dripped sufficiently from the other neck with the help of a dropper. This study was conducted in an inert atmosphere under a nitrogen gas flow of 200 min/mL. The suspension was continuously agitated on a magnetic stirrer at ambient temperature for 4 hours under a steady flow of nitrogen gas. Subsequently, the obtained mixtures were subjected to filtration, rinsed sequentially with ethanol and deionized water, and then dried in a

laboratory oven at 60°C for 12 h [21]. This process represents the reduction of Ag⁺ ions to Ag⁰ using hydrazine monohydrate as a reducing agent. In this study, chemical activation with ZnCl₂ was performed, and NPAgACs were produced by adding 1:0.5 and 1:1 ratios of AgNO₃ to activated carbons (ACs) carbonized at 700°C.

2.5. Characterization of produced AC and NPAgACs

Moisture, ash, and volatile matter determinations were made for the three mesh sizes, with the best efficiency of 12 different ACs for efficiency calculations. FT-IR analysis was conducted in the 4000–400 cm⁻¹ range to identify the functional groups in the HS, AC, and NPAgAC samples. The crystalline structures of AC and NPAgACs were examined using XRD analysis. SEM imaging was utilized to investigate the surface morphology of the samples. Surface characteristics including specific surface area (m²/g), average pore diameter (nm), and the volumes of micro-, meso-, and macropores (cm³/g) were evaluated through a multi-point Brunauer–Emmett–Teller (BET) analysis. The adsorption capacity was assessed using the iodine number method, a crucial technique for detecting micropores. The iodine number of activated carbon was determined using the sodium thiosulfate volumetric method, expressed in milligrams of iodine per gram of activated carbon [22, 23].

MB adsorption is a key analysis for evaluating the high porosity of AC. For this purpose, a 100 mg/L MB solution was prepared. Then, 0.1 g of AC was weighed, and 100 mL of the 100 mg/L MB solution was added. The mixtures were then agitated in an orbital shaker for 6 h. The obtained mixture was centrifuged at 1200 rpm, and samples were taken from the homogeneous supernatant, which was then measured using a UV-Vis spectrophotometer. The MB number of ACs was determined by calculating the adsorption capacity of the ACs.

2.6. Antimicrobial analysis of NPAg coated activated carbon (NPAgAC)

Well, the diffusion method was used to determine the antimicrobial effects of the prepared NPAgACs. In this study, two different pathogenic bacteria (*E. coli* and *S. aureus*) and two different antibiotic discs (Ampicillin 10 mg and Cefotaxime, used as the control) were employed. Stock bacterial cultures were transferred to a non-selective medium (PCA) and incubated at 36.5°C for 24 h. After incubation, isolated colonies were selected, and an inoculum was prepared. A ready-made saline solution was used to create the inoculum suspension. All experimental steps were conducted under a burner flame to ensure aseptic conditions and uphold proper sterilization protocols.

Several bacterial colonies with similar morphology were collected using a sterile cotton swab and suspended in a sterile saline solution (0.85% NaCl). The suspension density was adjusted to match the McFarland 0.5 standard, corresponding to approximately $1-2 \times 10^8$ CFU/mL of *E. coli*, using the Thermo Multiscan Go photometric device at a wavelength of 625 nm. Using a sterile cotton swab, the inoculum suspension was evenly spread across the agar surface in three directions. Following the EUCAST disc diffusion guidelines, the Petri dish was divided into equal sections, and wells with a diameter of 6 mm were created in each marked area using a sterile cork borer. Precisely weighed 10 mg of NPAgACs were placed into the prepared wells. On the other hand, the antibiotic discs used for antibiotic susceptibility comparison were placed on the agar surface and incubated at 36.5°C for 24 h. The results were classified as 'susceptible,' 'resistant,' or 'intermediate' for a given antibiotic based on the EUCAST disk diffusion breakpoint tables [24].

2.7. Time-dependent inhibition study of E coli using NPAgAC

To evaluate the adequate contact time and ideal temperature for NPAgACs in eliminating *E. coli* from potable water, the smear plate technique was employed. All procedures were performed within a sterile laminar flow cabinet and under flame to maintain aseptic conditions. The bacterial suspension was standardized to an

optical density of 625 nm, corresponding to the 0.5 McFarland standard (approximately 10^8 CFU/mL of *E. coli*). From this suspension, a 1 mL aliquot was withdrawn and further diluted by transferring it into 10 mL of sterile saline solution [25]. This process was repeated 3 times, corresponding to approximately $1-2 \times 10^5$ CFU/mL of *E. coli*. Then, 20 mg of NPAgAC2 was added to 10 mL of 10^5 CFU/mL suspension and incubated in a 150 rpm shaker at room temperature in an oxygenated environment, ensuring that no Ag-AC granules precipitated. The first moment of mixing, respectively, was assumed to be zero.

Subsequently, 0.1 mL of the diluted sample was transferred onto PCA medium at 10-minute intervals and evenly spread across the surface of the Petri dishes using a sterile disposable Drigalski spatula to achieve uniform distribution. The inoculated plates were prepared at four different temperature settings (20, 25, 30, and 35 °C) and assessed at three distinct exposure times (5, 10, and 15 minutes). All plates were incubated at 37 °C for 24 h, after which bacterial growth was quantified through colony counting, following the methodology outlined in references [26, 27].

The formula (1) below calculates the number of viable microorganisms, considering the dilution before sowing (1).

$$\frac{(CFU)}{mL} = \frac{(number\ of\ colonies) \times (dilution\ factor)}{culture\ plate\ volume} \quad (1)$$

3. Results and Discussion

3.1. Preliminary analysis results for hazelnut shell and activated carbon

ZnCl₂ was used as a chemical activation agent in this study because it is a frequently preferred chemical for producing activated carbon with a high surface area, is relatively inexpensive, and has a low carbonization temperature [28]. In the study, Activated carbons impregnated with HS, AC1 (50 mesh 1:1 ZnCl₂, AC2 (70 mesh 1:2 ZnCl₂), AC3 (150 mesh 1:3 ZnCl₂), and NPAg in two different ratios (0.5-1g) are encoded as NPAgAC1 and NPAgAC2. The experimental

results were determined by averaging the data from three repeat studies.

Upon examining the results of Table 1, the moisture content of the untreated hazelnut shell was calculated to be 6.05%. Upon reviewing the table, it was found that the hazelnut shells used in the study had a low ash content (1.64%), high volatile matter (71.1%), and a substantial fixed carbon content (21.21%). Raw materials with low ash content, high volatile matter, and high fixed carbon are preferred for producing activated carbon. A review of the literature shows that vegetable wastes with volatile matter content ranging from 20.40% to 67.36%, fixed carbon content between 17.62% and 70.70%, and ash content ranging from 0.3% to 5.0% are commonly used in activated carbon production [27, 29].

The literature indicates that the ash content of different biomass samples varies in the range of 0.1-38% [6, 30]. Compared to the literature, it has been observed that hazelnut shells can serve as a suitable starting material for the preparation of activated carbon, which can be used as an adsorbent due to their low ash content [31]. When the moisture, ash, and volatile matter content of the activated carbons are examined, it is found that the values fall within the ranges of 1.89% to 3.1%, 1.1% to 1.4%, and 4.8% to 7.3%, respectively. It is suitable for producing activated carbon in every mesh range of hazelnut shells with low ash content [30]. It is known that pores are formed in the structure of activated carbon due to the effect of the activation agent used, and a significant portion of the existing ash content of the activated carbon is removed from the structure after production [30, 31]. The ash content may be higher in activated carbons, in which $ZnCl_2$, which has a micropore size, is the agent due to the possibility of the inorganic structure being trapped in these pores [32]. The results are consistent with studies on producing activated carbon from hazelnut shells [33, 34]. Table 2 shows the elemental analysis results for HS, AC1, AC2, and AC3.

Table 1. Activated carbon proximate analysis results

(dry basis (%))	HS	AC1	AC2	AC3	Method
Yield	-	43	40	37	-
Moisture	6.05	1.89	2.2	3.1	ASTM D 2016 2.67
Ash	1.64	1.4	1.8	1.1	ASTM D1102 0.17
Volatile Matter	71.1	7.3	6.2	4.8	ASTM E 872 78.50
Fixed carbon	21.21	89.41	89.8	91	By difference

Table 2. HS and AC elemental analysis results (LECO Instruments, USA)

Raw Material Name	%C	%H	%N	%S	%O*
HS	49.348	6.0992	0.36148	0,048	44.144
AC1	64.244	2.225	0.658	0.043	32.893
AC2	70.240	0.815	0,482	0.002	28.461
AC3	69.583	0.196	0.721	0.004	29.496

As seen in Table 2, when HS is converted into activated carbon, the C content increases while the O content decreases. This result is considered quite successful for all three samples.

3.2. Characterization results of AC and NPAgACs

The number of Iodine and MB, SBET, t-plot Micropore, t-plot, Vtotal, Vmicro, and Average pore size (\AA) for AC1, AC2, AC3, NPAgAC1, NPAgAC2 are determined, and the results are given in Table 3.

When the results in Table 3 were examined, the MB values obtained for three activated carbons were 490-499 mg/g. It was observed that the mesopores of the produced ACs played a vital role in the adsorption of large adsorbate molecules, including dye molecules [32]. The study observed that $ZnCl_2$, a preferred chemical activation agent, is highly successful in activating the raw material. In the study, the results of the iodine number analysis, performed to investigate the adsorption of small molecules onto AC, were found to be in the range of 1142-1612 mg/g. The iodine number of NPAgACs decreased to 934-1022 mg/g due to the reduction in pore volume and surface area caused by the

binding of silver (Ag) particles. When Ag nanoparticles are incorporated into the activated carbon structure, they tend to occupy or block some of the micropores, which are primarily responsible for iodine adsorption. As a result, the overall accessibility of these micropores to iodine molecules diminishes, leading to a lower iodine number [34, 35]. This decline indicates a reduction in the material's adsorption capacity for small molecules like iodine, which is often used as an indicator of microporosity. These results showed parallelism with the BET surface area.

Many other researchers have obtained similar results to those presented here, demonstrating a parallel relationship between the BET surface area and the iodine number [34- 36]. Based on the IUPAC classification, pores larger than 500 Å are called macropores, pores ranging from 500 to 20 Å are considered mesopores, and pores smaller than 20 Å are categorized as micropores. This study observed that three activated carbons had a mesoporous structure with a pore size of 21-25 Å [37, 38]. In addition, when the BET surface areas were evaluated for three different mesh sizes in the study, the highest surface area was observed in the 150-mesh size in AC3, confirming the increase in surface area as the particle size decreased [39]. The decrease in the MB, Iodine, and BET surface area of NPAgACs is related to the attachment of NPAg ions to the surface area and is an expected result. The decrease in surface area, especially, proves that activated carbon adsorbs NPAg ions. An increase in surface area was observed in only one sample, which was attributed to the increased porosity in the structure resulting from the process performed in an inert atmosphere during the impregnation of NPAg ions into the activated carbon [37].

3.3. SEM and EDS results of AC and NPAgACs

In Figure 1, AC1 (50 mesh 1:1 ZnCl₂), AC2 (70 mesh 1:2 ZnCl₂), and AC3 (150 mesh 1:3 ZnCl₂)

are shown. The SEM and EDS images indicate that the EDS images exhibit amorphous structures resembling the typical honeycomb-activated carbon morphology, with well-developed porous textures and irregular surface features.

As for the SEM images of Figure 1. a) AC1, b) AC2, and c) AC3 are examined at 1000x magnification. It is observed that the surface structure has undergone significant changes, resulting in a porous structure, after the raw material was chemically activated with ZnCl₂ and carbonized at high temperatures in a N₂ atmosphere. When the EDS results are examined, it is seen that the carbon ratio in the structure increases as the raw material size decreases. The amount of carbon in the raw material, which is approximately 45% on average, rises to 81% after chemical activation and carbonization, indicating that most of the oxygen, hydrogen, and volatile substances in the structure are removed during these processes.

The particle size of the raw material affects the pore structure and pore volume of the activated carbon produced. It is stated that when working with small particle sizes, large surface areas and pore volumes are obtained [21]. As the raw material's particle size decreased, the porous structure and the carbon content increased significantly. This indicates that the smaller particle size enables better interaction and more efficient impregnation of the chemical substance into the raw material, thereby enhancing the overall surface area and porosity of the material. The improved impregnation process ensures better incorporation of the active component, which is essential for achieving the desired properties in the final material.

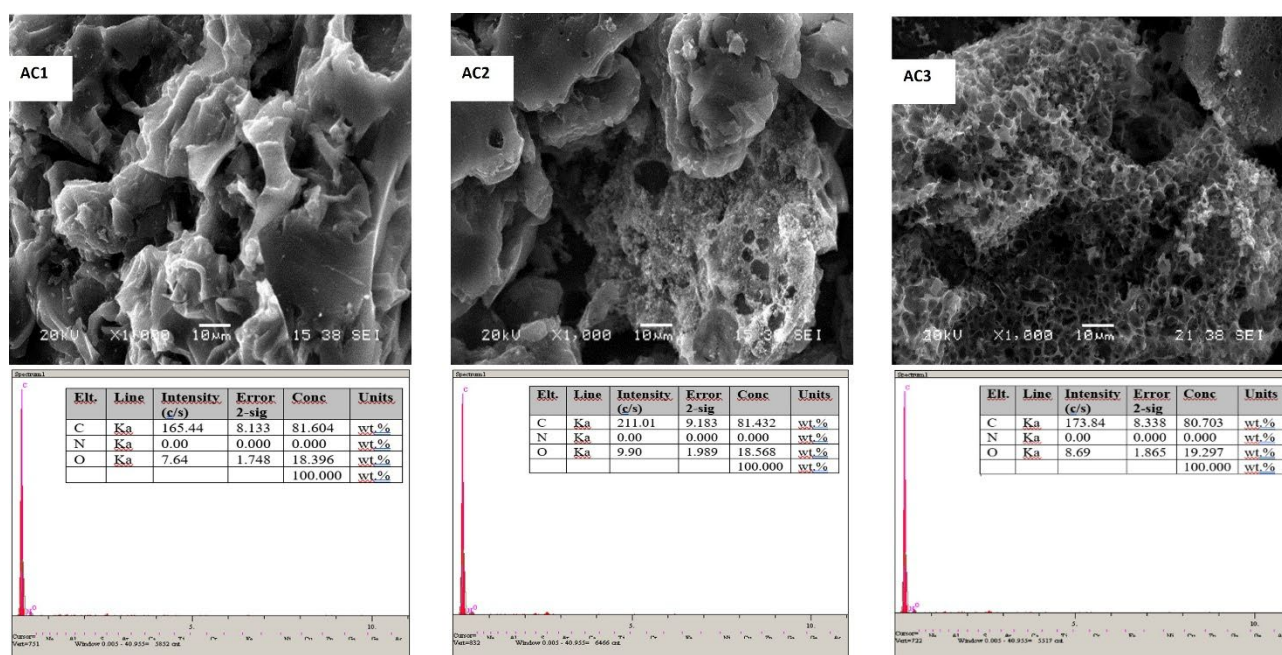


Figure 1. SEM images of a) AC1, b) AC2, c) AC3 at 1000x magnification

3.4. NPAGAC1 and NPAGAC2 SEM and EDS results

Figure 2 shows SEM and EDS images of NPAGAC1 and NPAGAC2. The bright silver appearance is remarkable after NPAG binds to the active carbon. The SEM images (Figure 2), NPAGAC1 and NPAGAC2, were obtained by impregnating two different amounts (0.5-1g) of NPAG on 50 mesh AC1, whose chemical activation was performed at a 1:1 ratio with $ZnCl_2$. It is seen that the silver particles are bright and dispersed on the surface of the activated carbon. When the images are compared, a) 0.5 g NPAG is added in NPAGAC1 and less, b) NPAGAC2 silver ions are seen more brightly

because 1 g NPAG is impregnated into the structure. It was observed that the ACs we obtained bind NPAG at a high rate due to their porous structure and high surface area. The EDS analyses further confirm the presence of silver at the elemental level, consistent with the SEM observations.

These findings align well with previously reported literature, which similarly emphasizes the affinity of activated carbon for incorporating metal nanoparticles due to its textural properties and surface chemistry [40, 41].

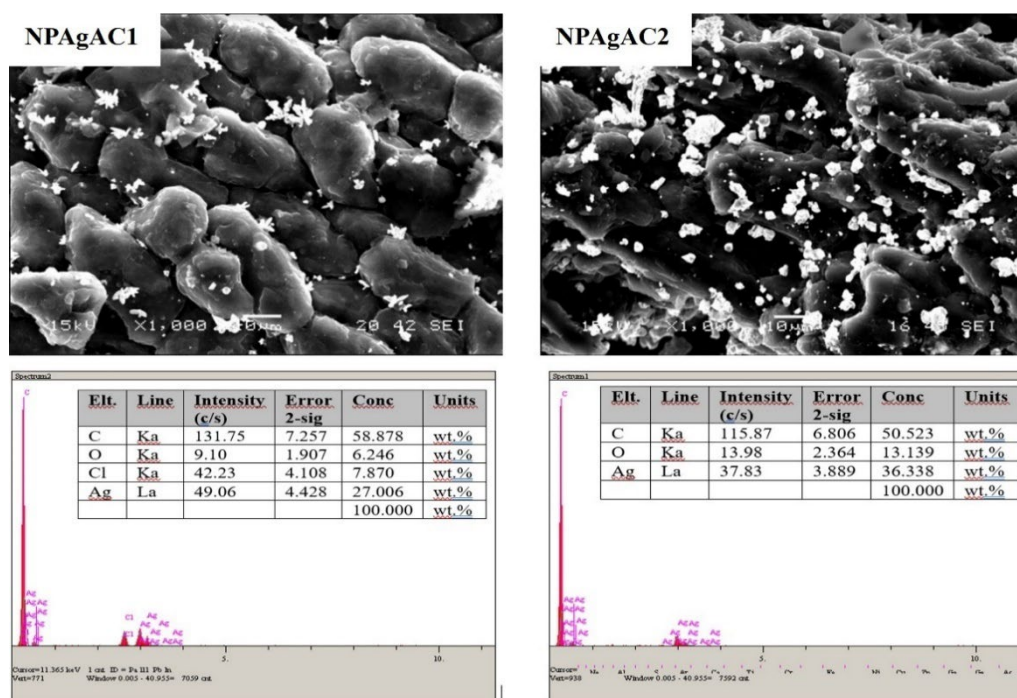


Figure 2. SEM images of a) NPAgAC1, b) NPAgAC2, at 1000x magnification

When the EDS (Figure 3) analyses of the samples were compared at 1000x magnification, the carbon ratio in AC1 was 81%, while it decreased to 58% in NPAgAC1 and 50% in NPAgAC2. This is because of the increase in Ag⁺ ions bound to the structure. The amount of silver in the structure increases linearly as the amount retained on the surface increases.

3.4. AC1, AC2 and AC3 XRD results

Figure 3 below shows the XRD images for AC1 (50 mesh, 1:1 ZnCl₂), AC2 (70 mesh, 1:2 ZnCl₂), and AC3 (150 mesh, 1:3 ZnCl₂). The images' typical amorphous structure and harmony prove that the study was done correctly.

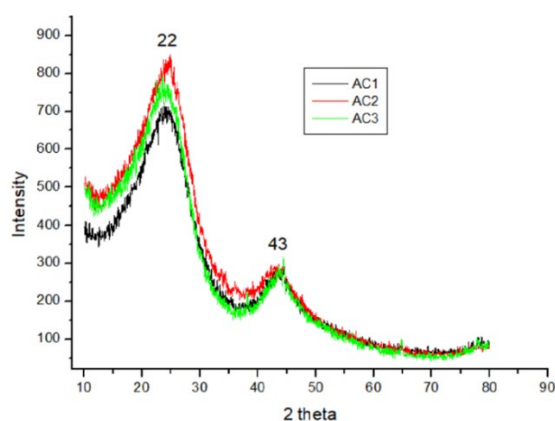


Figure 3. AC1, AC2 and AC3 XRD image

When the XRD results of AC1, AC2, and AC3, as shown in (Figure 4), are examined, it is evident that the synthesized activated carbons exhibit the same degree of spectrum across the three different mesh intervals. This indicates that the study was conducted precisely and the results are accurate. Results at 22° and 43°, with typical peaks at 2 θ , indicate the amorphous structure of activated carbon. These broad peaks are typically attributed to the (002) and (100) planes of disordered graphitic carbon layers, indicating a lack of long-range crystalline order. Additionally, it was observed that the mesh size difference did not affect the amorphous structure of the activated carbon during production. These results are consistent with existing literature, which also reports similar broad peaks in chemically or thermally activated carbon materials, affirming their non-crystalline, highly porous nature [21].

3.5. NPAgAC1 and NPAgAC2 XRD results

The XRD images of NPAgAC1 and NPAgAC2 given in (Figure 4) showed that the study performed by overlapping the NPAg-bound ACs at two different rates was consistent in nanoparticle binding.

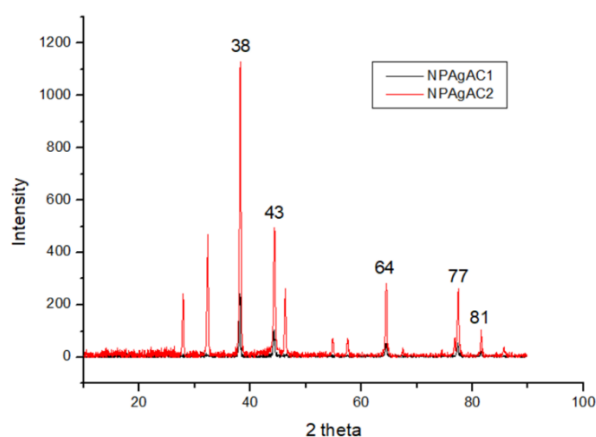


Figure 4. NPAgAC1 and NPAgAC2 XRD image

In Figure 4, the XRD analysis results for NPAgAC1 and NPAgAC2, as shown in the figure, are examined. Sharp peaks are observed at 2θ angles of 38° , 43° , 64° , 77° , and 81° . These peaks obtained as a result of the analysis belong to surface-centered metallic silver in the coordinates (111), (200), (220), (311), and (222). No silver oxide peaks were observed in the XRD results, which were supported by the literature [21, 42]. After adding silver, the amorphous structure of the activated carbons transformed into a crystalline structure, as indicated by the sharpness of the peaks.

3.6. AC1, AC2 and AC3 FT-IR results

Figure 5 shows FT-IR images for AC1 (50 mesh 1:1 ZnCl_2), AC2 (70 mesh 1:2 ZnCl_2), and AC3 (150 mesh 1:3 ZnCl_2). The harmony of the images proves that the study was done correctly.

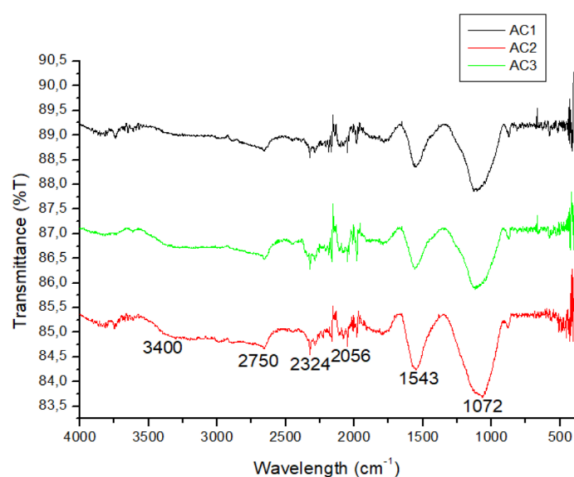


Figure 5. AC1, AC2 and AC3 FT-IR image

When Figure 5 examines the IR spectra of activated carbon in three different mesh sizes obtained by ZnCl_2 activation of the raw material, it is observed that the results are very similar to each other within each mesh range. Upon examining the spectra, it was observed that the four significant peaks required evaluation and interpretation. The prominent OH stretch vibration peak at 3400 cm^{-1} in the hazelnut shell has disappeared. The structure's moisture is dehydrated during the activation agent chemicals and carbonization. Peaks between 2056 and 1543 cm^{-1} indicate the presence of carboxylic acid and/or lactone groups. The peak at 1072 cm^{-1} corresponds to the C-O stretching mode in the heterocyclic rings. The peaks between 2056 and 2750 cm^{-1} are the aliphatic C-H stretch. The stresses observed in the study are consistent with the typical image of activated carbon [43].

3.7. NPAgAC1 and NPAgAC2 FT-IR results

Figure 6 presents the FT-IR spectra of NPAgAC1 and NPAgAC2, obtained after incorporating NPAg into the produced activated carbon at two different rates. These spectra offer valuable insights into the structural and chemical modifications that occur on the activated carbon surface upon the addition of NPAg. The observed variations in functional groups and bonding characteristics further confirm the successful incorporation of NPAg at different concentrations, highlighting its potential impact on the material's physicochemical properties.

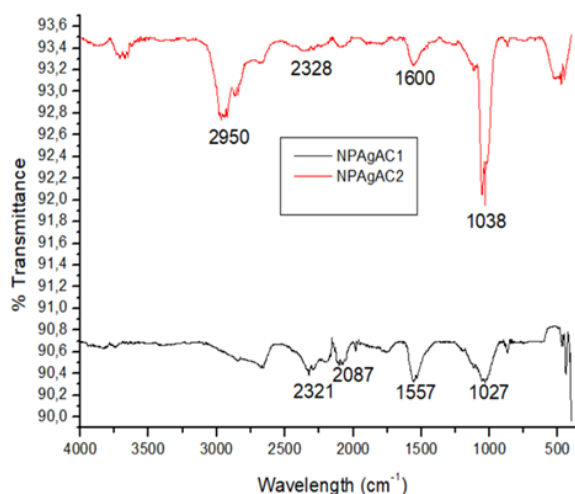


Figure 6. NPAgAC1 and NPAgAC2 FT-IR image

When Figure 6, the peak bands of the graph of NPAGAC1 and NPAGAC2 shown in (Figure 7) are 1027-1038 cm^{-1} , 1557-1600 cm^{-1} , 2328-2321 cm^{-1} , and 2950 cm^{-1} with the tensile vibration of C = C bending (alkene) peak bands such as amine groups (C-N), aromatic carbon-carbon double bonds (C = C), carbon dioxide bonds (O = C = O) and alcohol bond (O-H, strong intermolecular bond), strong carbon-carbon confirmed the formation of double bonds (aromatic and alkene bonds). Peaks at 2950 cm^{-1} , 1557-1600 cm^{-1} , and 1027-1038 cm^{-1} indicate that Ag⁺ ions combine with activated carbons through reduction [44, 45].

3.8. Antimicrobial results of NPAGACs

3.8.1. Well diffusion results

Figure 7 illustrates the wide zone diameters formed due to the antimicrobial well diffusion study conducted using NPAG-coated activated carbons. This study was carried out to evaluate the antimicrobial efficacy of the synthesized materials against two bacterial strains, *E. coli* and *S. aureus*.

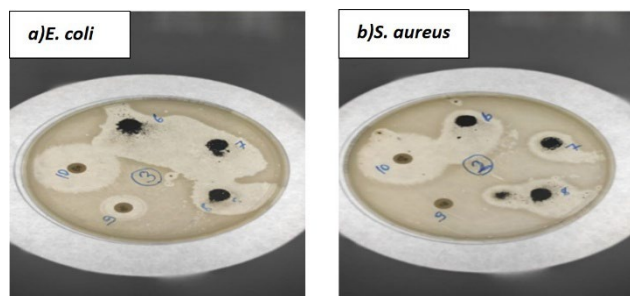


Figure 7. a) *E. coli* and b) *S. aureus* Zone diameters formed in the presence of NPAGAC and antibiotics

6) AC/NPAGAC 7) 0.5gNPAGAC 8) 1gNPAGgAC 9)10mg Ampicillin 10) 30mg Cefotaxim

S. aureus can be found as a part of the normal microbiota in the skin, upper respiratory tract, and intestinal mucosa of all warm-blooded animals, including humans. *S. aureus* is extremely important, as it is a pathogenic risk factor in respiratory tract infections and a significant concern in food safety. It is a

microorganism with high mortality rates, especially in hospital infections with methicillin-resistant (MRSA) strains [46]. In our study, antibiotic resistance was confirmed, and the zone diameters (20-21 mm) observed in the Petri dishes indicated the effectiveness of the antimicrobial agent (Table 3). Consumption of water contaminated with *E. coli*, in particular, is one of the major causes of waterborne human infections [47]. Waterborne diarrheal disease causes 2 million deaths worldwide each year, mostly in children under 5 years of age [48]. *E. coli*, which is considered an indicator pathogen for drinking water, appears to be effectively inhibited by the NPAGAC produced in the study.

Table 3. Zone diameters measured for *E. coli* and *S.*

Sample	<i>Aureus</i>	
	<i>S. aureus</i>	<i>E. coli</i>
6)AC/NPAGAC	20 mm	20 mm
7)0.5gNPAGAC	18 mm	18 mm
8)1gNPAGgAC	21 mm	17 mm
9)10 mgAmpisilin	0 (18)*mm	11(14)*mm
10)30 mg Cefotaxim	30 mm	27 mm

The zone diameter difference between 0.5 g and 1 g is very low in NPAGACs, which act as actively as the third-generation cephalosporin group antibiotics used as the control group in the study (Table 3). This demonstrated that adding 0.5 g of NPAG has a sufficient effect in removing pathogenic bacteria, and there is no need to use more silver, which is an expensive product, especially in terms of cost.

3.9. Results of time- and temperature-dependent inhibition of NPAGAC2 classes of *E. coli*

Figure 8 shows the results of the smear plate method used to determine the inhibition of *E. coli* with the produced NPAGAC2 at different temperatures and at various time intervals.

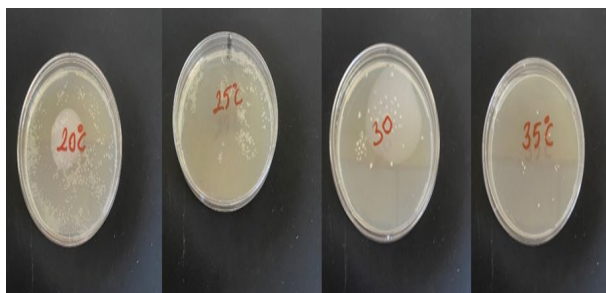


Figure 8. Time- and temperature-dependent inhibition of *E. coli* in the presence of NPAGAC2

As seen in (Figure 9), since NPAGAC1 was added to the suspension diluted to approximately $1-2 \times 10^5$ CFU/mL *E. coli* by the Smear plate method and mixed, 0.1 ml samples were taken and planted in Petri dishes, the initial number of microorganisms was $1-2 \times 10^6$ CFU/mL. Colony counts were performed in 12 Petri dishes after 24 hours of incubation at 36.5°C for bacteria cultivated at four different temperatures (20, 25, 30, and 35°C) and at three different time intervals (5, 10, and 15 minutes).

The Colony (*E. coli*) Count according to Time and Temperature is shown in Figure 10. In this study, which aimed to determine the effects of both time and temperature on the inhibition of microorganisms, the number of colonies and the logarithmic numerical expression of live microorganisms are presented in Figure 10. The analysis compared the number of colonies over time, specifically up to the 15th minute, for each experimental condition. In these experiments, an initial microbial concentration of approximately $1-2 \times 10^6$ CFU/mL was used across four different temperature settings. When the microbial counts were evaluated, it was observed that the most significant decrease in colony numbers occurred at 25°C, indicating that this temperature had the most potent inhibitory effect on microbial survival within the given timeframe.

Furthermore, when the correlation values were examined, it was found that the R^2 values were high for all tested temperatures, demonstrating a strong statistical relationship between time and microbial reduction. The consistently high R^2 values across different conditions suggest that the study's findings are reliable and that the

experimental methodology was appropriately designed to assess microbial inhibition. These results further emphasize the critical role of temperature in determining microbial viability over time and highlight the significance of understanding thermal inactivation patterns in microbial control applications.

Figure 11 shows the pattern of change in the growth (Log) of the starting microorganisms as a function of temperature and time.

When Figure 11 is examined, it is seen that the temperature-dependent inhibition of *E. coli* with an initial concentration of 10^6 CFU/mL increases over time. The death of microorganisms due to the effect of heat generally follows first-order reaction kinetics. In the first-order rate expression, the death rate is proportional to the current concentration of the component. Since the initial concentration is equal here, the effect of time on temperature was measured. When the results were examined, the correlation values were calculated as $R^2 = 0.9338$, $R^2 = 0.9541$, $R^2 = 0.9434$, and $R^2 = 0.9641$ for temperatures of 20, 25, 30, and 35 °C, respectively. The highest correlation and activation value was observed at 35 °C. It has been seen in.

As illustrated in Figure 11, the initial D-values of microorganisms tend to vary significantly depending on both temperature and exposure duration. This observed variation underscores the significant role of environmental conditions, particularly heat, in influencing microbial resistance and survivability. As the temperature increases, the D-value generally decreases, indicating that microorganisms become less resistant to thermal treatment. Conversely, at lower temperatures, higher D-values suggest a greater tolerance to heat, requiring longer exposure times to achieve the same level of microbial reduction. The relationship between D-value, temperature, and time provides valuable insights into optimizing thermal treatment processes for microbial control applications. The textural characteristics, MB adsorption capacities, and iodine numbers of the synthesized

activated carbon and its silver-loaded derivatives (NPAgACs) are comprehensively summarized in Table 4 to evaluate their surface properties and overall adsorption performance. The iodine number indicates microporosity, while MB adsorption capacity reflects the mesoporous structure and surface interaction potential.

Comparing these values between pristine activated carbon and NPAgAC samples reveals how silver nanoparticle loading affects the material's structure and adsorption efficiency. This comparison offers key insights into the relationship between surface properties and performance, guiding the selection of effective adsorbents for specific applications.

Table 4. MB, Iodine number, and textural properties of activated carbon and NPAgACs

Sample	Number of MB (mg/g)	Number of Iodine (mg/g)	S _{BET} (m ² /g)	t-Plot Micropore (m ² /g)	t-Plot (m ² /g)	V _{total} (cm ³ /g)	V _{micro} (cm ³ /g)	Average pore size (Å)
AC1	499	1237	1334	399.441	933.573	0.846	0.186	25.392
AC2	492	1612	1264	488.960	775.351	0.688	0.231	21.773
AC3	490	1047	1506	558.925	947.504	0.822	0.260	21,834
NPAgAC1	453	1022	1517	631.154	886.757	0.747	0.305	19.704
NPAgAC2	421	934	1178	456.710	721.339	0.621	0.215	21.112

As shown in Table 4, a comparative summary of the MB adsorption capacity, iodine number, and key textural properties, including surface area and pore structure, of pristine activated carbon and silver nanoparticle-impregnated activated carbons (NPAgACs) is presented. The MB adsorption capacity reflects the material's ability to remove dye molecules from aqueous solutions, primarily indicating the availability of mesopores. The iodine number is a classical indicator of microporosity and total surface area. A noticeable variation in these parameters is observed upon NPAg loading.

Typically, a slight decrease in both iodine number and surface area after Ag impregnation suggests partial pore blockage or surface coverage by silver nanoparticles. Nevertheless, the retained or even enhanced MB adsorption in some NPAgACs indicates that the functional surface chemistry may have improved due to the presence of silver, supporting dye molecule interaction. These results highlight the trade-off between surface area reduction and functional enhancement through silver nanoparticle incorporation.

Table 5 presents the number of surviving microorganisms and their corresponding D-values following the inhibition of *E. coli* by NPAgAC2 under varying temperature and time conditions. This data provides insight into the thermal resistance behavior of *E. coli* in the presence of the silver-loaded activated carbon, offering a quantitative evaluation of the antibacterial efficiency of NPAgAC2 over time.

When Table 5 is examined, the temperature with the highest D value is 30 °C. However, when the results were evaluated, 30°C proved unsuitable for inhibiting *E. coli*, and 20 °C was found to be the most suitable temperature.

Table 5. Number and D values of microorganisms surviving in the medium after inhibition of *E. coli* by temperature and time-dependent on NPAgAC2

Temperature °C – (log)				
Time(mn)	20 °C	25 °C	30 °C	35 °C
0	6	6	6	6
5	2.466	2.444	2.201	1.724
10	2.423	2.103	1.968	1.204
15	2.264	1.68	1.41	0.95
D (mn)	0.0202	0.0755	0.0997	0.0774

The Colony (*E. coli*) Count according to Time and Temperature is shown in Figure 10. This study calculated D values to determine the heating time required to kill 90% of the live microorganism population in the environment at four different temperatures. The results were 0.0202 for 20°C, 0.0755 for 25°C, 0.0997 for 30°C, and 0.0774 for 35 °C. Upon examination of Table 5, the temperature with the highest D value is 30°C. However, upon evaluation of the results, 30°C proved unsuitable for inhibiting *E. coli*, and 20°C was found to be the most suitable temperature.

Figure 11 demonstrates that *E. coli* inhibition is time- and temperature-dependent, with lower D-values indicating higher sensitivity. At 20°C, the lowest D-value (0.0202) corresponds to a 90% reduction in bacterial numbers per minute with

NPAgAC1. Figure 11 further supports this trend, showing strong correlations ($R^2 = 0.901-0.9954$) between Log D-values and time across different temperatures. The highest correlation was observed at 25 °C, indicating a strong linear relationship between Log D and time at this temperature.

These results align well with Figure 11, confirming the study's consistency, reliability, and overall validity. Furthermore, the findings suggest that 25°C and 15 min were sufficient to effectively eliminate *E. coli* from drinking water, demonstrating the rapid antimicrobial properties of the developed materials. The NPAgACs in this study were deemed highly effective in inhibiting *E. coli*, as strongly supported by existing literature [26, 2

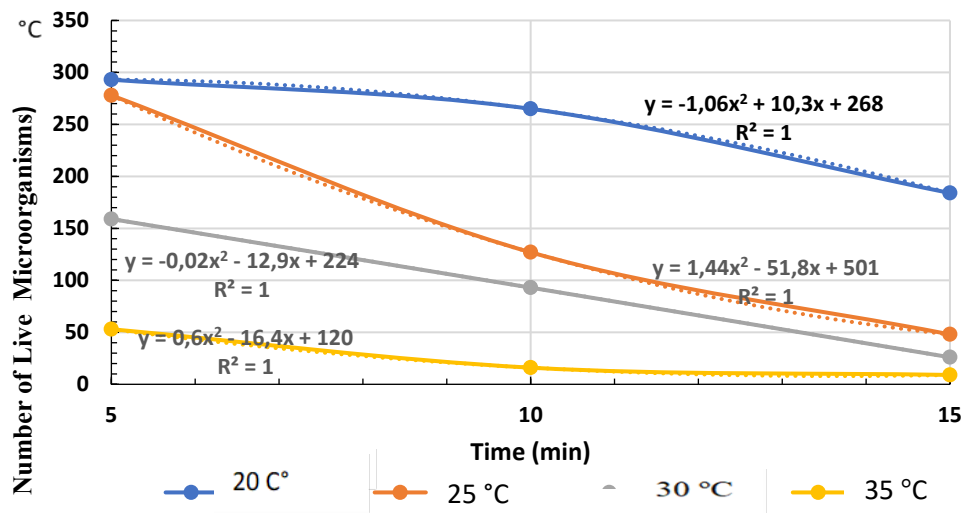


Figure 9. Time and temperature decreased colony (*E.coli*) number

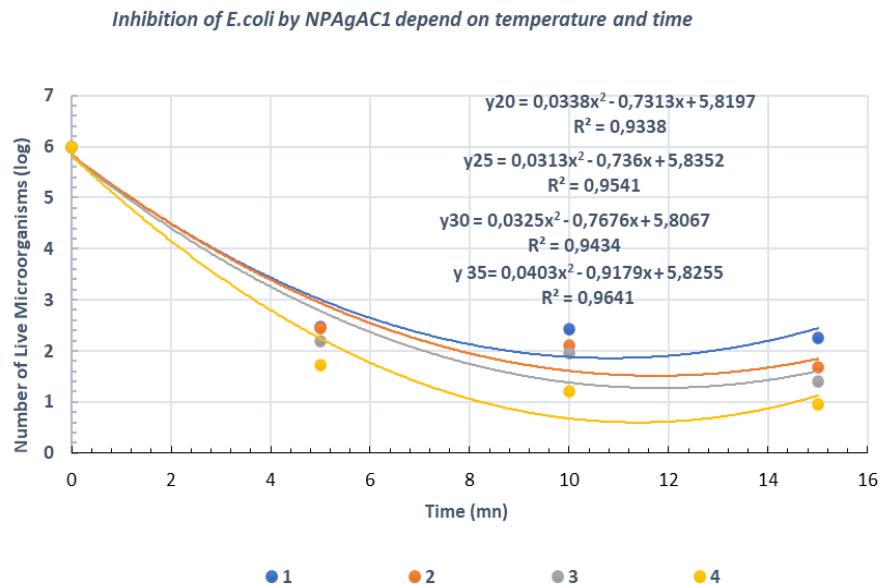


Figure 10. Change in the number of living microorganisms (log) depends on temperature and time

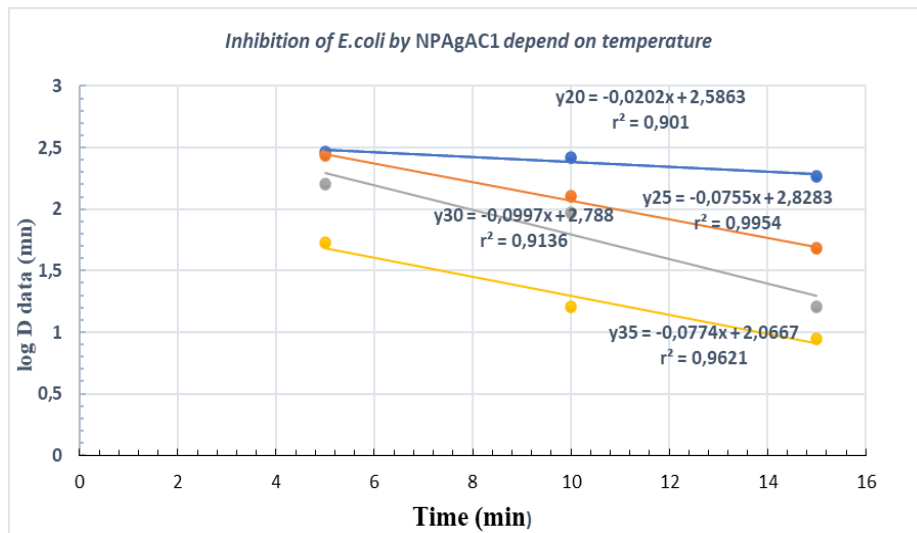


Figure 11. Inhibition of *E.coli* by NPAGAC1 depends on temperature

4. Conclusion

In this study, NPAGAC was obtained by binding NPAG to activated carbon produced from hazelnut shells, an agricultural waste, to address and remove dyestuff and microbial pollution in waters, which pose a risk to food safety and public health. The antimicrobial activity and dye removal of the obtained NPAGACs were tested and found suitable for removing *E.coli* from polluted waters. Three different sizes (50, 70, 150 mesh) of hazelnut shells are obtained by carbonizing the hazelnut shells in an inert nitrogen (N₂) atmosphere at 700 °C in a thermal tube furnace, for three of which the best efficiency is obtained (AC1, 50 mesh 1:4 (43%),

AC2, 70 mesh 1:2 (40%), and AC3, 150 mesh 1:3 (37%) characterization studies were performed.

SEM, FT-IR, and BET images were evaluated, revealing a honeycomb porous structure of activated carbon with a high surface area. Yield analysis showed the highest yield at 43%. The MB number of the produced ACs was 490-499 mg/g, while the iodine number ranged from 1047 to 1612 mg/g, consistent with the BET surface area. While the MB numbers of NPAGACs ranged from 421 to 453 mg/g, the iodine numbers decreased to 934-1022 mg/g due to the reduction in pores resulting from Ag binding. The BET surface area for ACs was 1264-1506 m²/g, while for NPAGACs, it was determined to be 1178-

1517 m²/g. Well-diffusion and spreading plate methods were used to control the antimicrobial properties of NPAGAC. *Escherichia coli* (*E. coli*) and *Staphylococcus aureus* (*S. aureus*), which are considered risk factors for food safety and public health, were used as pathogenic microorganisms in the study. In the study, two different antibiotic discs (Ampicillin 10 mg and cefotaxim 30 mg) were used in the control group, and the results were determined to be highly effective according to EUCAST criteria. In addition, when the study of *E. coli* in drinking water was evaluated at three time points (5, 10, 15 min) and four different temperatures (20, 25, 30, and 35°C), 15 min at 25 °C was found to be sufficient. The hazelnut shell is a suitable starting material for raw carbon production, and NPAGAC exhibits high antimicrobial properties about food safety.

Article Information Form

Authors' Contribution

Birsen Sarıcı conducted the experiments and interpreted the microbiological studies. Esra Altıntığ carried out the characterization studies, interpretation, and manuscript writing. Şükrü Karataş supervised the manuscript and contributed to the experimental interpretations.

The Declaration of Conflict of Interest/ Common Interest

No conflict of interest or common interest has been declared by authors.

Artificial Intelligence Statement

No artificial intelligence tools were used while writing this article.

Copyright Statement

Authors own the copyright of their work published in the journal and their work is published under the CC BY-NC 4.0 license.

References

- [1] J. Baruah, B.K. Nath, R. Sharma, S. Kumar, R.C. Deka, D. C. Baruah, E. Kalita, "Recent Trends in the Pretreatment of Lignocellulosic Biomass for Value-Added Products," *Front Energy Res*, vol. 6, no. 141, pp. 1-19, 2018.
- [2] T. Q. Tuan, N. Van Son, H. T. K. Dung, H. L. Nguyen, T. T. Bui, T. V. A. Nguyen, D. H. Nguyen, H. H. Nguyen, "Preparation and properties of silver nanoparticles loaded in activated carbon for biological and environmental applications," *Journal Hazard Mater*, vol. 192, no. 3, pp. 1321-1329, 2011.
- [3] A. A. Mostafa, A. A. Al-Askar, K. S. Almaary, T. M. Dawoud, E. N. Sholkamy, M. M. Bakri, "Antimicrobial activity of some plant extracts against bacterial strains causing food poisoning diseases," *Saudi Journal of Biological Sciences*, vol. 25, no. 2, pp. 361-366, 2018.
- [4] A. Mani, M. Amalanathan, M. S. M. Mary, C. Parvathiraja, A. Alothman, S. M. Wabaidur, M. A. Islam, "Enhanced photocatalytic and biological observations of green synthesized activated carbon, activated carbon doped silver, and activated carbon/silver/titanium dioxide nanocomposites," *Journal of Inorganic Organometallic Polymers Materials*, vol. 32, no. 1, pp. 267-279, 2022.
- [5] W. Trisunaryanti, K. Wijaya, T. Riyono, N. Wahyuningtyas, S. P. Utami, L. Larasati, "Characteristics of coconut shell-based activated carbon as Ni and Pt catalyst support for hydrotreating Calophyllum inophyllum oil into hydrocarbon-based biofuel," *Journal of Environmental Chemical Engineering*, vol. 10, no. 5, pp. 108-209, 2022.
- [6] A. Sobhan, K. Muthukumarappan, L. Wei, T. Van Den Top, R. Zhou, "Development of an activated carbon-based nanocomposite film with antibacterial property for smart food packaging," *Materials Today Communications*, vol. 23, pp. 101-m124, 2020.
- [7] J. C. M. Márquez, A. H. Partida, M. del Carmen, M. Dosta, J. C. Mejía, J. A. B. "Martínez Silver nanoparticles applications (AgNPS) in aquaculture," *International Journal of Fisheries and Aquatic Studies*, vol. 6, pp. 5-11, 2018.

- [8] S. Yorgun, D. Yıldız, "Preparation and characterization of activated carbons from Paulownia wood by chemical activation with H_3PO_4 ," *Journal of the Taiwan Institute of Chemical Engineers*, vol. 53, pp. 122-131, 2015.
- [9] H. Teramura, E. Yasuda, Y. Naisei, "Impact of Spreading Time to Recovery Rate in Suitability Test of Solid Agar Media," *Biocontrol Science and Technology*, vol. 26, no. 1, pp. 43-47, 2021.
- [10] N. Söyler, J. L. Goldfarb, S. Ceylan, M. T. Saçan, "Renewable fuels from pyrolysis of *Dunaliella tertiolecta*: An alternative approach to biochemical conversions of microalgae," *Energy*, vol. 120, pp. 907-914, 2017.
- [11] H. Ç. Kazıcı, V. Yönten, M. R. Kivanç, M. Ertas, F. Salman, M. Yayla, "Antimicrobial properties of multimetallic of silver compounds immobilized on active carbon and nano carbon tubes," *Current Research in Green and Sustainable Chemistry*, vol. 4, pp. 100-204, 2021.
- [12] K. S. Ukanwa, K. Patchigolla, R. Sakrabani, E. Anthony, S. Mandavgane, "A review of chemicals to produce activated carbon from agricultural waste biomass," *Sustainability*, vol. 11, no. 22, p. 6204, 2019.
- [13] T. V. Duncan, "Applications of nanotechnology in food packaging and food safety: Barrier materials, antimicrobials, and sensors," *Journal of Colloid and Interface Science*, vol. 363, no. 1, pp. 1-24, 2011.
- [14] S. Moeinzadeh, E. Jabbari, "Nanoparticles and their applications. In Springer handbook of nanotechnology," Springer, Berlin, Heidelberg, pp. 335-361, 2017.
- [15] U. Latif, K. Al-Rubeaan, A. T. Saeb, "A review on antimicrobial chitosan-silver nanocomposites: A roadmap toward pathogen targeted synthesis," *International Journal of Polymeric Materials and Polymeric Biomaterials*, vol. 64, no. 9, pp. 448-458, 2015.
- [16] A. A. El-Sayed, A. M. Khalil, M. El-Shahat, N.Y. Khaireldin, S.T. Rabie, "Antimicrobial activity of PVC-pyrazolone-silver nanocomposites," *Journal of Macromolecular Science, Part A*, vol. 53, no. 6, pp. 346-353, 2016.
- [17] P. Chingombe, B. Saha, R. J. Wakeman, "Sorption of atrazine on conventional and surface modified activated carbons," *Journal of Colloid and Interface Science*, vol. 302, no. 2, pp. 408-416, 2006.
- [18] B. Sarıcı, Ş. Karatas, E. Altıntig, "Removal of Methylene blue from aqueous solution with activated carbon produced from hazelnut shells by K_2CO_3 activation," *Desalination and Water Treatment*, vol. 254, pp. 287-301, 2022.
- [19] Y. Zhao, Z.O. Wang, X. Zhao, W. Li, S. X. Liu, "Antibacterial action of silver-doped activated carbon prepared by vacuum impregnation," *Applied Surface Science*, vol. 266, pp. 67-72, 2013.
- [20] S. Singh, A. Bharti, V. K. Meena, "Structural thermal zeta potential and electrical properties of disaccharide reduced silver nanoparticles," *Journal of Materials Science: Materials in Electronics*, vol. 25, pp. 3747-52, 2014.
- [21] C. G. Giske, J. Turnidge, R. Cantón, G. Kahlmeter, "Update from the European committee on antimicrobial susceptibility testing (EUCAST)," *Journal of Clinical Microbiology*, vol. 60, no. 3, pp. e00276-21, 2022.
- [22] Y. Sudaryanto, S. B. Hartono, W. Irawaty, H. Hindarso, S. Ismadji, "High Surface area activated carbon prepared from cassava peel by chemical activation," *Bioresource Technology*, vol. 97, pp. 734-739, 2007.

- [23] M. Uyttendaele, E. Franz, O. Schlüter, "Food safety, a global challenge," *International Journal of Environmental Research and Public Health*, vol. 13, no. 1, p. 67, 2016.
- [24] P. Biswas, R. Bandyopadhyaya, "Water disinfection using silver nanoparticle-impregnated activated carbon: *Escherichia coli* cell-killing in batch and continuous packed column operation over a long duration," *Water Research*, vol. 100, pp. 105-115, 2016.
- [25] S. Thomas, R.A. Gonsalves, J. Jose, S. H. Zyoud, A. R. Prasad, J. Garvasis, "Plant-based synthesis, characterization approaches, applications and toxicity of silver nanoparticles: A comprehensive review," *Journal of Biotechnology*, vol. 394, pp. 135-149, 2024.
- [26] Y. Baran, H. S. Gökçe, M. Durmaz, "Physical and mechanical properties of cement containing regional hazelnut shell ash wastes," *Journal of Cleaner Production*, vol. 259, p. 120965, 2020.
- [27] Ö. Bağ, K. Tekin K. "Atık lignoselülozik biyokütleden hidrotermal karbon üretimi ve karakterizasyonu," *Gazi Üniversitesi Mühendislik Mimarlık Fakültesi Dergisi*, vol. 35 no. 2, pp. 1063-1076, 2019.
- [28] X. Jian, X. Zhuang, B. Li, X. Xu, Z. Wei, Y. Song, E. Jiang, "Comparison of characterization and adsorption of biochars produced from hydrothermal carbonization and pyrolysis," *Environmental Technology & Innovation*, vol. 10, pp. 27-35, 2018.
- [29] Z. Heidarinejad, M. H. Dehghani, M. Heidari, G. Javedan, L. Ali, M. Sillanpää, "Methods for preparation and activation of activated carbon: A review," *Environmental Chemistry Letters*, vol. 18, no. 2, pp. 393-415, 2020.
- [30] Ç. Çuhadar, "Production and characterization of activated carbon from hazelnut shell and hazelnut husk," (Master's thesis, Middle East Technical University), pp. 23-82, 2005.
- [31] E. Altıntığ, B. Sarıcı, S. Karataş, "Prepared activated carbon from hazelnut shell where coated nanocomposite with Ag⁺ used for antibacterial and adsorption properties," *Environmental Science and Pollution Research*, vol. 30, no. 5, pp. 13671-13687, 2023.
- [32] D. Angın, E. Altıntığ, T. E. Köse, "Influence of process parameters on the surface and chemical properties of activated carbon obtained from biochar by chemical activation," *Bioresource Technology*, vol. 148, pp. 542-549, 2013.
- [33] C. Tang, Y. W. Sun, "Green and facile fabrication of silver nanoparticles loaded activated carbon fibers with long-lasting antibacterial activity," *RSC advances*, vol. 4, no. 2, pp. 523-530, 2014.
- [34] K. Y. Yoon, J. H. Byeon, C. W. Park, J. Hwang, "Antimicrobial effect of silver particles on bacterial contamination of activated carbon fibers," *Environmental Science & Technology*, vol. 42, no. 4, pp. 1251-1255, 2008.
- [35] T. C. Chandra, M. M. Mirna, Y. Sudaryanto, S. J. C. E. J. Ismadji, "Adsorption of basic dye onto activated carbon prepared from durian shell: Studies of adsorption equilibrium and kinetics," *Chemical Engineering Journal*, vol. 127, no. 1-3, pp. 121-129, 2007.
- [36] A. G. Blanco, J. A. de Oliveira, R. López, J. C. Moreno-Piraján, L. Giraldo, G. Zgrablich, K. Sapag, "A study of the pore size distribution for activated carbon monoliths and their relationship with the storage of methane and hydrogen. *Colloids and Surfaces A*," *Physicochemical and Engineering*, vol. 357, no. 1-3, pp. 74-83, 2010.
- [37] N. Korkmaz, A. Ceylan, Hamid, A. Karadağ, A. S. Bülbül, M. N. Aftab, O. Cevik, F. Sen, "Biogenic silver nanoparticles synthesized via *Mimusops elengi* fruit extract, a study on antibiofilm, antibacterial, and anticancer activities,"

- Journal of Drug Delivery Science and Technology, vol. 59, p. 101864, 2010.
- [38] M. A. Islam, M. V. Jacob, E. Antunes, "A critical review on silver nanoparticles: From synthesis and applications to its mitigation through low-cost adsorption by biochar," *Journal of Environmental Management*, vol. 28, p. 1111918, 2021.
- [39] Ş. Karadirek, H. Okkay, "Ultrasound assisted green synthesis of silver nanoparticle attached activated carbon for levofloxacin adsorption," *Journal of the Taiwan Institute of Chemical Engineers*, vol. 105, pp. 39-49, 2019.
- [40] E. Altintig, S. Kirkil "Preparation and properties of Ag-coated activated carbon nanocomposites produced from wild chestnut shell by ZnCl₂ activation," *Journal of Taiwan Institute of Chemical Engineers*, vol. 63, pp. 180-188, 2016.
- [41] S. Sharifan, "A comparative optimization study of activated carbon production from hazelnut shells by thermal and microwave heating methods," (Doctoral dissertation, Imperial College London), pp. 212-231, 2014.
- [42] E. Altintig, O. F. Soydan, "Methylene blue adsorption and preparation silver bound to activated carbon with sol-gel method," *Sakarya University Journal of Science*, vol. 22, no. 6, pp. 1812-1819, 2018.
- [43] L. Y. Le, F. Baron, M. Gautier, "Staphylococcus aureus and food poisoning," *Genetics and Molecular Research: GMR*, vol. 2, no. 1, pp. 63-76, 2003.
- [44] H. B. Haberecht, N. J. Nealon, J. R. Gilliland, A. V. Holder, C. Runyan, R. C. Opper, E. P. Ryan, "Antimicrobial-resistant *Escherichia coli* from environmental waters in Northern Colorado," *Journal of Environmental and Public Health*, vol. 2019, pp. 1-13, 2019.
- [45] M. A. Lim, J. Y. Kim, D. Acharya, B. B. Bajgain, J. H. Park, S. J. Yoo, K. Lee, "A diarrhoeagenic enteropathogenic *Escherichia coli* (EPEC) infection outbreak that occurred among elementary school children in Gyeongsangbuk-Do province of South Korea was associated with consumption of water-contaminated food items," *International Journal of Environmental Research and Public Health*, vol. 17, no. 9, pp. 1-19, 2020.
- [46] A. Yurtay, M. Kılıç, "Fast and effective production of industrial grade activated carbon," *Journal of Porous Materials*, vol. 30, pp. 1207-1220, 2023.
- [47] S. Konyalı, M. Demir, "The agricultural policies applied for hazelnut and problems of hazelnut producers in Sakarya Province," *Eurasian Journal of Agricultural Economics*, vol. 4, no. 1, pp. 11-21, 2024.
- [48] M. A. Kara, "Investigation of hazelnut producing provinces with cluster analysis methods," *Ordu University Journal of Science and Technology*, vol. 14, no. 2, pp. 396-410, 2024.